Supporting Information

Unveiling the role of hydrothermal carbon dots as anodes in sodium-ion batteries with ultrahigh initial Coulombic efficiency

Fei Xie,[a,b] Zhen Xu,[a] Anders C. S. Jensen,[a,b] Feixiang Ding,[d] Heather Au,[a] Jingyu Feng,[a] Hui Luo,[a,c] Mo Qiao,[a] Zhenyu Guo,[a] Yaxiang Lu,[d] Alan J. Drew,[b] Yong-Sheng Hu[d] and Maria-Magdalena Titirici*[a]

[a] Department of Chemical Engineering, Imperial College London, London, SW7 2AZ, UK

[b] School of Physics and Astronomy, Queen Mary University of London, London, E1 4NS, UK

[c] School of Engineering and Materials Science, Queen Mary University of London, London, E1 4NS, UK

[d] Beijing Key Laboratory for New Energy Materials and Devices, Beijing National Laboratory for Condensed Matter Physics, Institute of Physics, Chinese Academy of Sciences, Beijing, 100190, China

*Correspondence: m.titirici@imperial.ac.uk

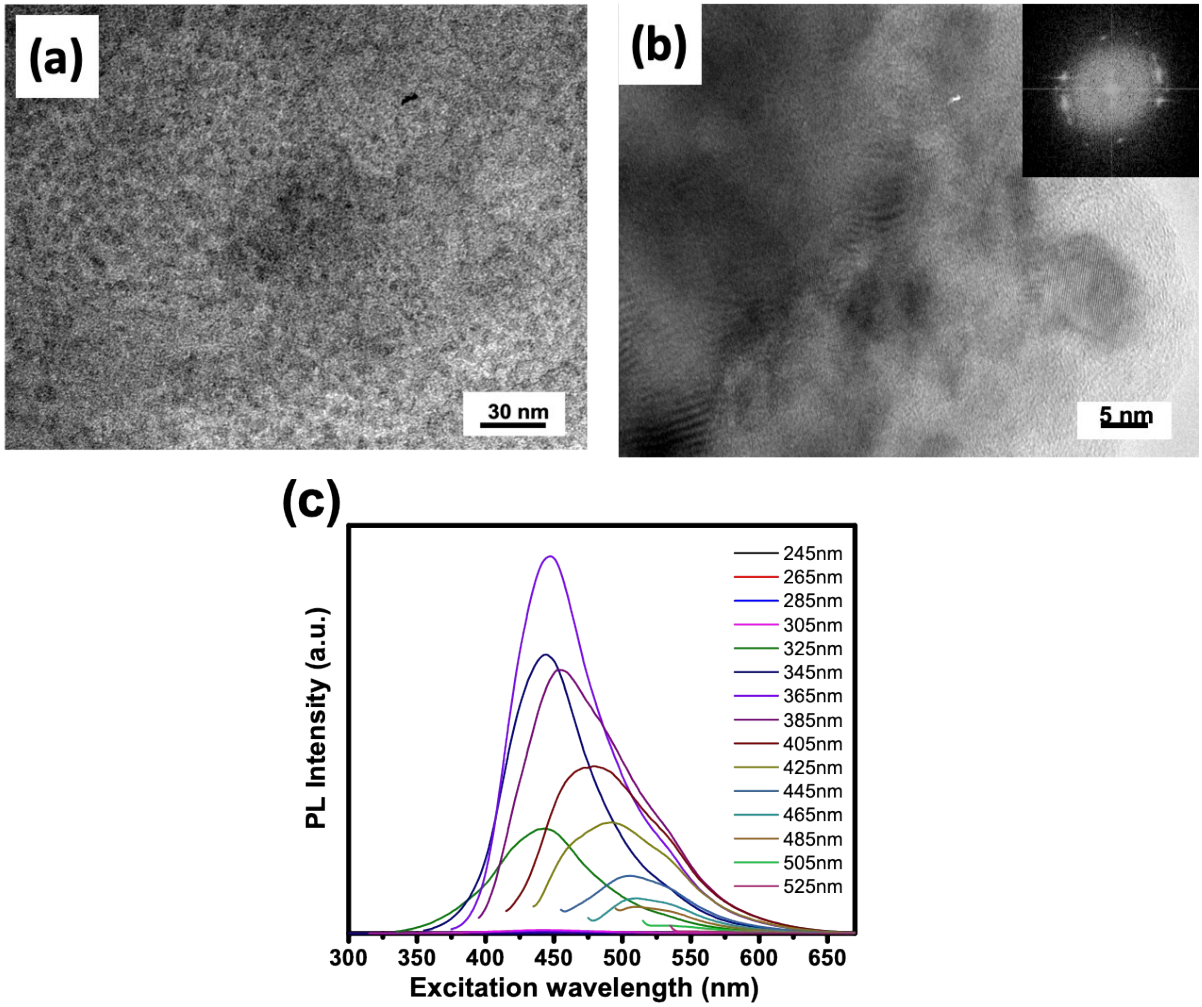

Fig. S1 (a) TEM image of CCD at low magnification showing the individual carbon dots embedded on the amorphous carbon layer. (b) TEM image of aggregated CCD at high magnification showing some crystalline nanodomains (inset is the FFT graph showing the crystallinity). (c) Fluorescence spectra of CCD in liquid phase.

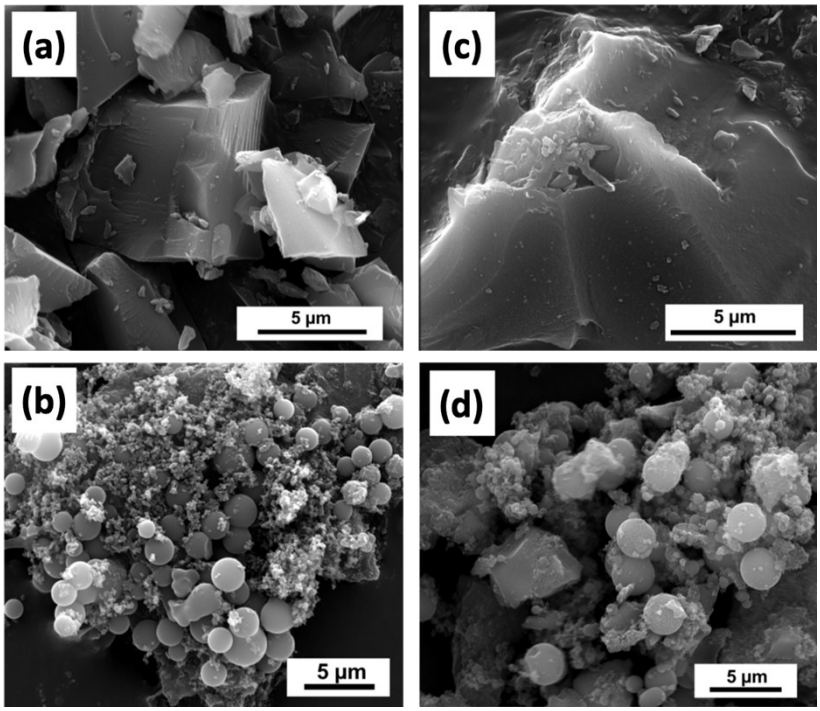

Fig. S2 SEM images of (a) CCD1000. (b) CHTC1000. (c) CCD1500. (d) CHTC1500.

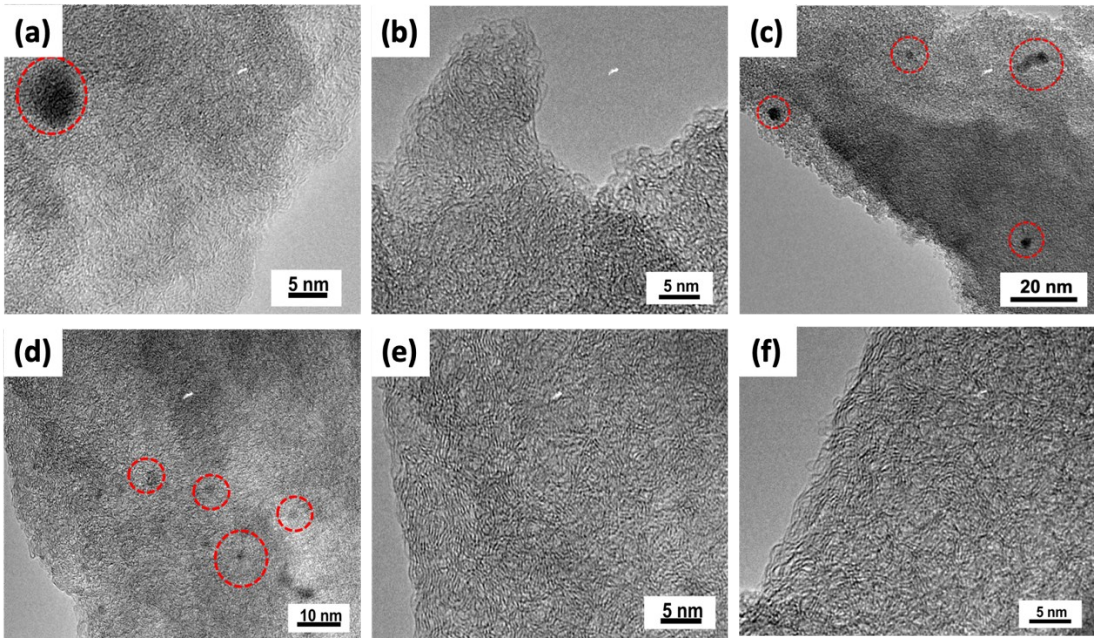

Fig. S3 TEM images showing the turbostratic nanodomains and the remained carbon dots (in the red circles) of (a) CCD1000. (b) CHTC1000. (c) CCD1300. (d)-(e) CCD 1500. (f) CHTC1500.

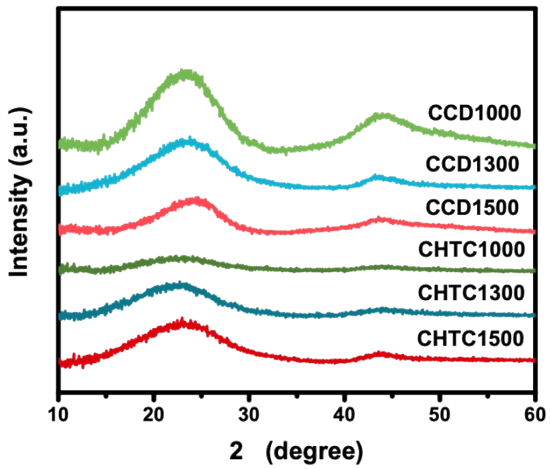

Fig. S4 XRD patterns of CCD and CHTC carbonized at different temperatures.

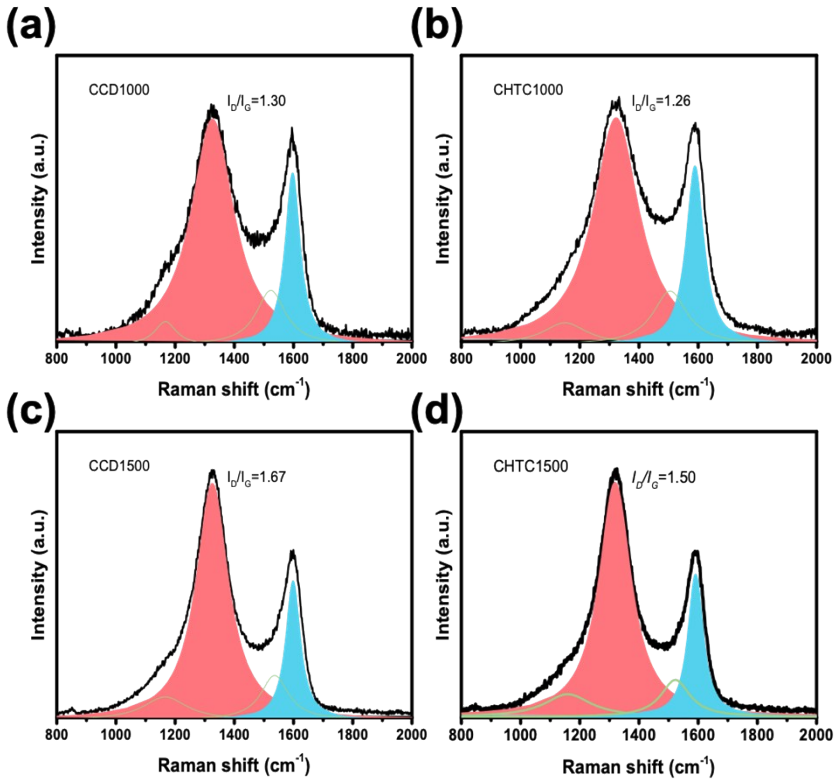

Fig. S5 Raman spectra of CCD and CHTC carbonized at 1000 °C and 1500 °C

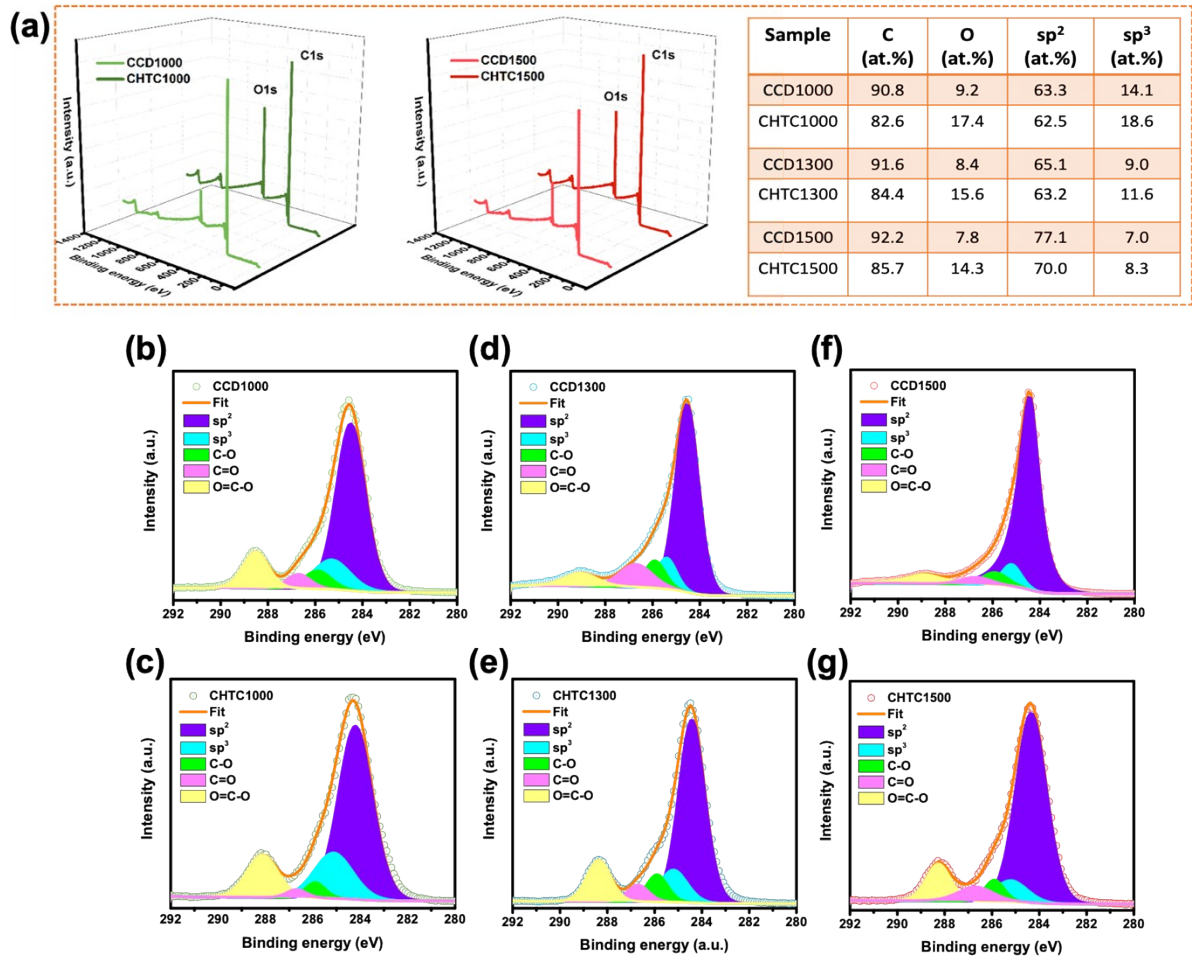

Sample	C (at.%)	O (at.%)	sp^2 (at.%)	sp^3 (at.%)
CCD1000	90.8	9.2	63.3	14.1
CHTC1000	82.6	17.4	62.5	18.6
CCD1300	91.6	8.4	65.1	9.0
CHTC1300	84.4	15.6	63.2	11.6
CCD1500	92.2	7.8	77.1	7.0
CHTC1500	85.7	14.3	70.0	8.3

Fig. S6 (a) XPS Survey of CCD and CHTC at 1000 and 1500 °C. The table on the right shows the element contents of all the obtained carbon materials. Fitted C1s spectra of (b) CCD1000. (c) CHTC1000. (d) CCD1300. (e) CHTC1300. (f) CCD1500 and (g) CHTC1500.

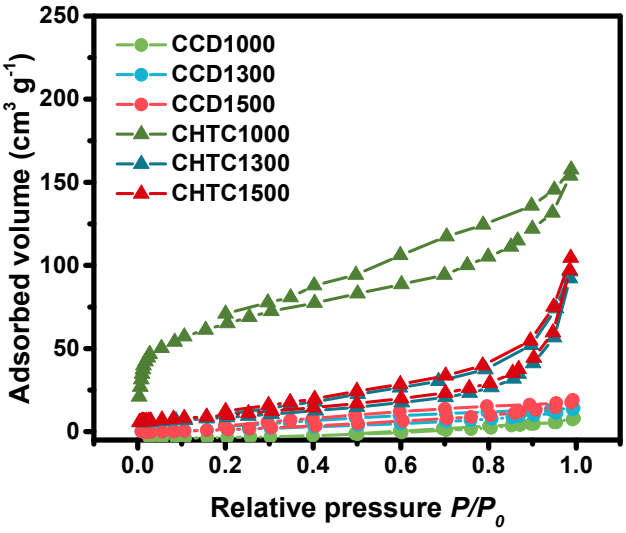

Fig. S7 N_2 adsorption isotherms of carbonized CCD and CHTC at different temperatures.

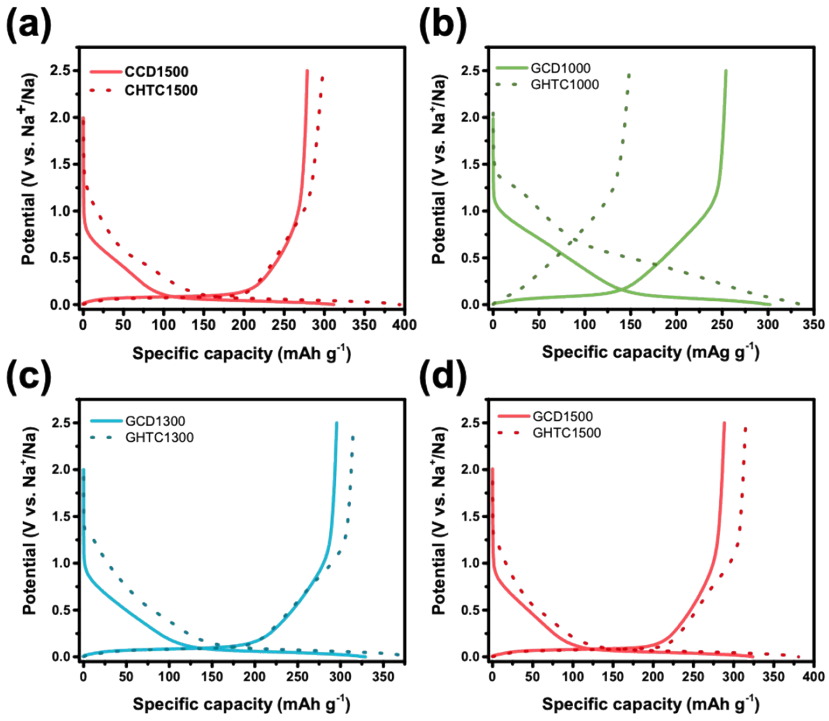

Fig. S8 Initial galvanostatic discharge/charge profiles at 30 mA g^{-1} of (a) CCD1500 and CHTC1500. (b)-(d) glucose-derived carbon dots (GCD) and glucose-derived HTC carbon (GHTC) carbonized at 1000, 1300 and 1500 °C.

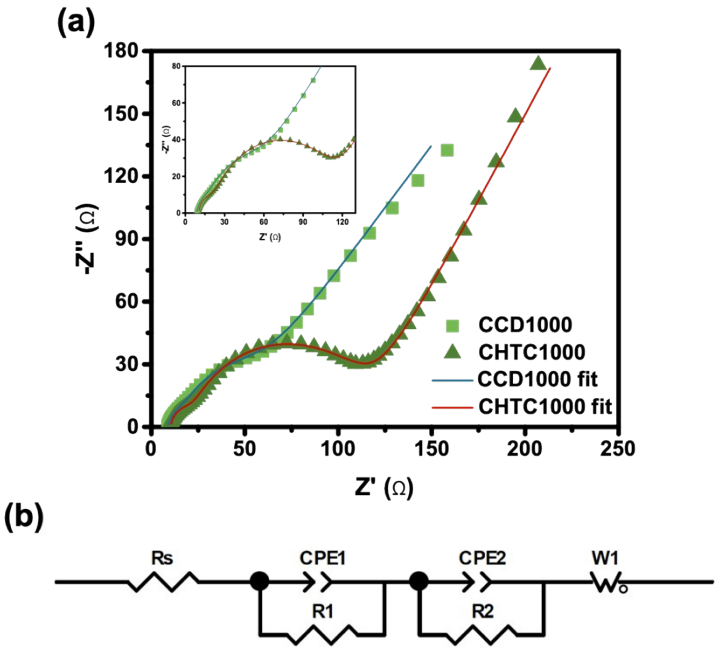

Fig. S9 (a) Nyquist plot of CCD1000 and CHTC1000 after the initial cycle (semi-circles inset). (b) Equivalent circuit.

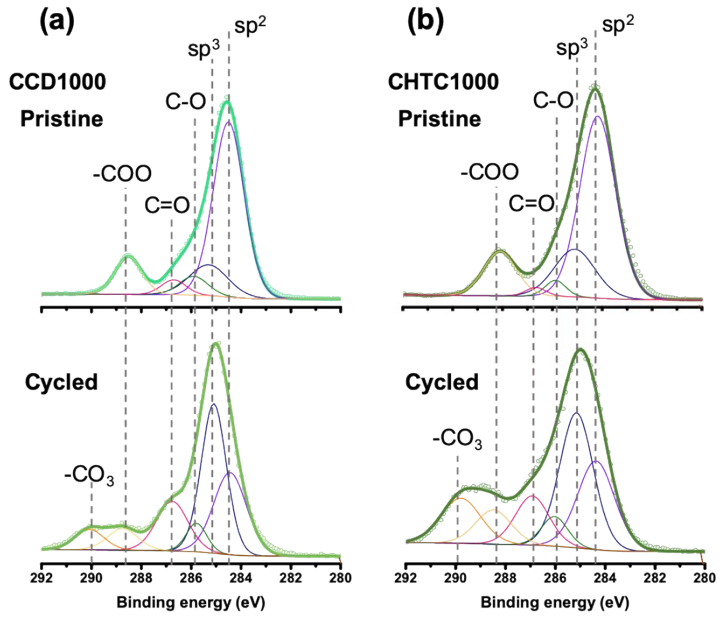

Fig. S10 C1s spectra from the XPS results of pristine and cycled (a) CCD1000 and (b) CHTC1000.

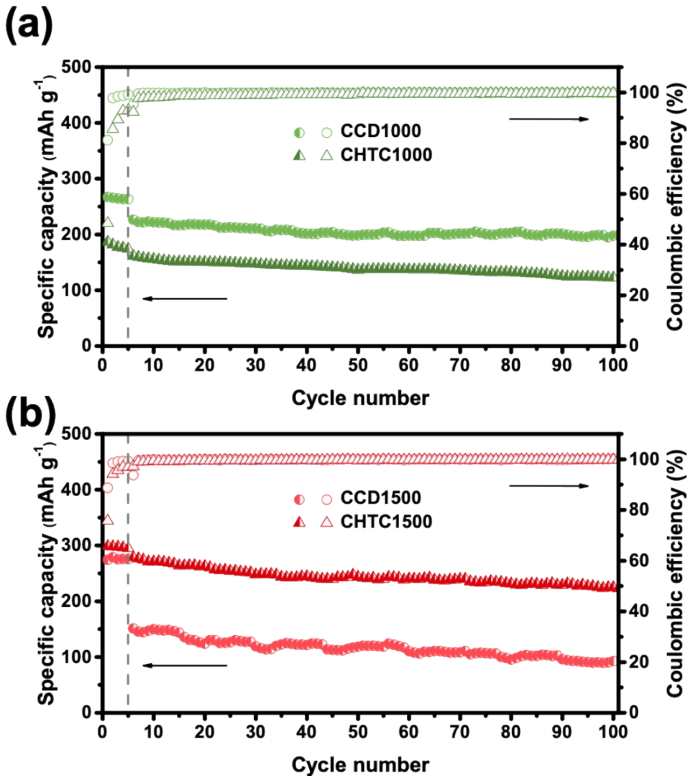

Fig. S11 Cycling performance of CCD and CHTC at (a) 1000 °C and (b) 1500 °C at 150 mA g^{-1} (first five cycles are performed at 30 mA g^{-1}) in half cell.

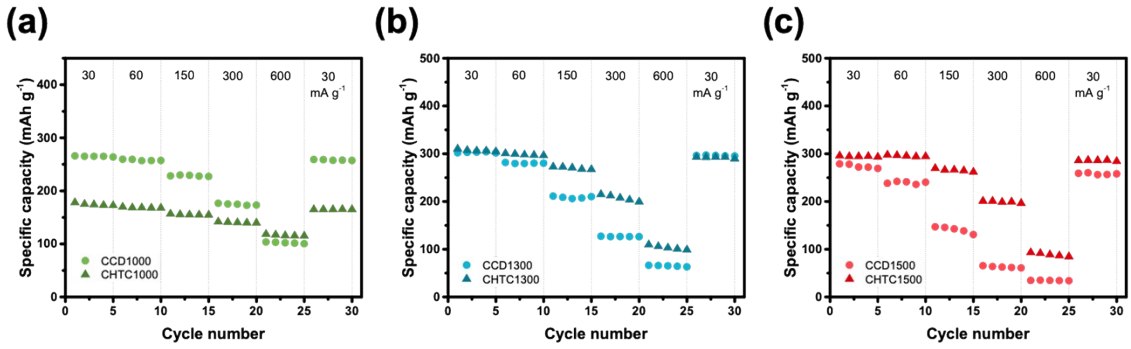

Fig. S12 Rate capability of carbonized CCD and CHTC at (a) 1000 °C. (b) 1300 °C and (c) 1500 °C in half cell. Current densities are from 30 to 600 mA g^{-1}.

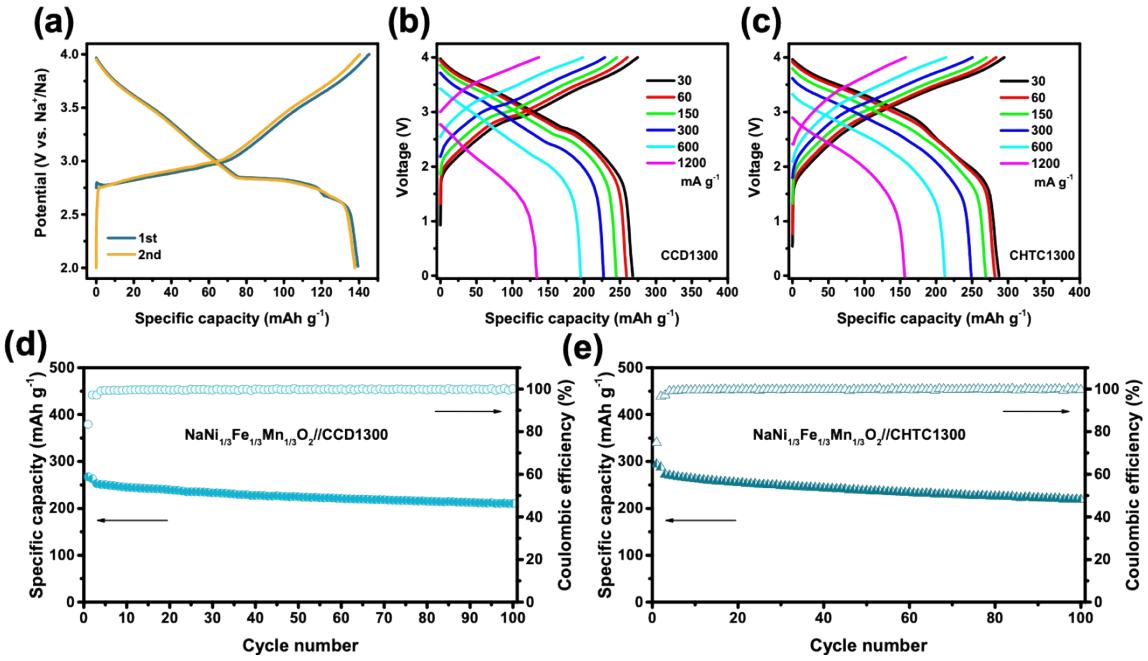

Fig. S13 (a) Galvanostatic charge/discharge profiles of $NaNi_{1/3}Fe_{1/3}Mn_{1/3}O_2$ cathode in half cell at current density of 14 mA g^{-1}. (b)-(c) Typical charge/discharge curves at different current densities of CCD1300 and CHTC1300 in full cell from 30 to 1200 mA g^{-1} . (d)-(e) Cycling performance of CCD1300 and CHTC1300 at 60 mA g^{-1} in full cell (the first two cycles are activated at 30 mA g^{-1}).

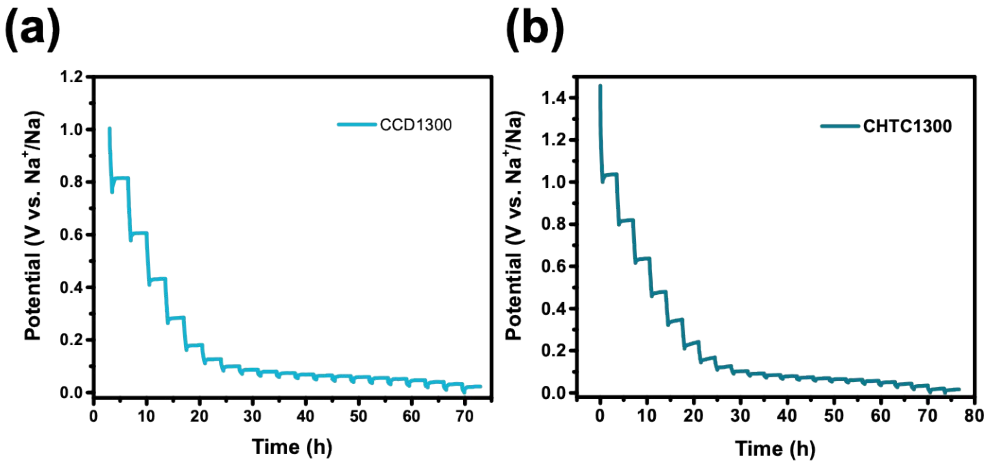

Fig. S14 Typical GITT potential profiles of (a) CCD1300 and (b) CHTC1300.

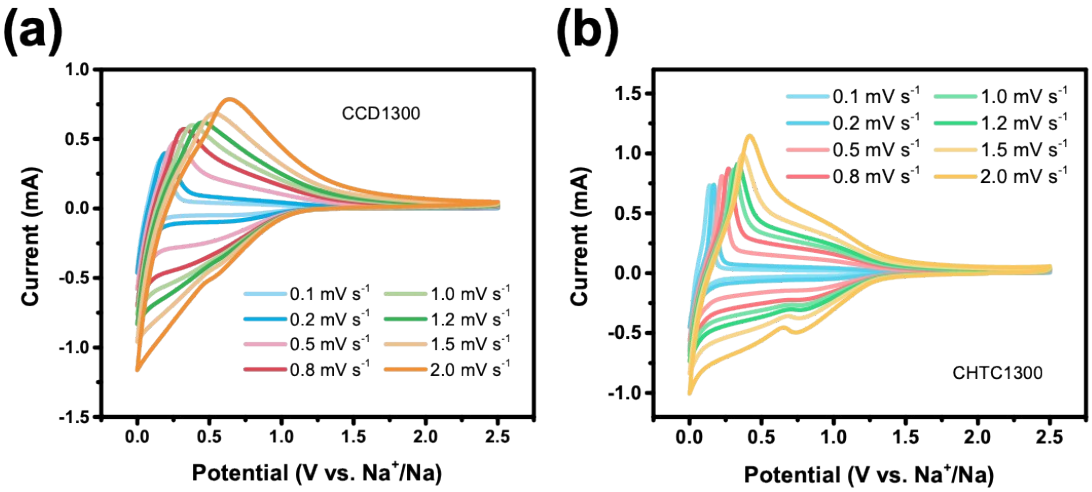

Fig. S15 CV curves at various scan rates of (a) CCD1300 and (b) CHTC1300.

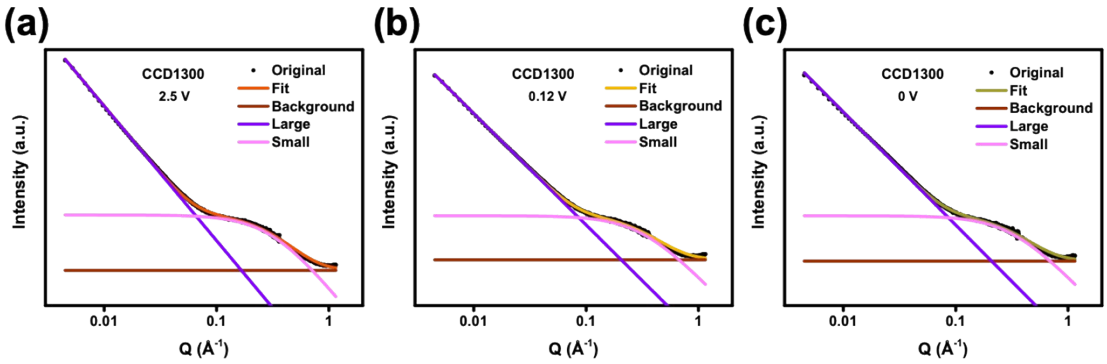

Fig. S16 Fitted ex situ SAXS patterns of CCD1300 at the second discharge process from 2.5 to 0 V (vs. Na^+/Na).

Table S1 Physical parameters of carbonized CCD and CHTC.

Sample	d_{002} (Å)	FWHM$_{002}$[a] (degree)	I_D/I_G
CCD1000	3.84	8.41	1.30
CHTC1000	3.94	9,70	1.26
CCD1300	3.77	7.72	1.58
CHTC1300	3.92	8.78	1.34
CCD1500	3.71	7.39	1.67
CHTC1500	3.81	7.87	1.62

[a]FWHM002: Full width at half maximum of (002) peaks.

Table S2 Pore structure parameters of carbonized CCDs and CHTCs.

Sample	S_{BET}[a] ($m^2\ g^{-1}$)	A_{SAXS}[b] (10^{-6})	B_{SAXS}[c]	Pore diameter[d] (nm)
CCD1000	5	0.97	0.0032	1.72
CCD1300	10	0.90	0.0051	1.96
CCD1500	12	0.80	0.0047	2.34
CHTC1000	232	87.74	0.0050	1.62
CHTC1300	34	40.54	0.0050	1.65
CHTC1500	40	42.89	0.0041	2.00

[a] BET surface area from N_2 adsorption.

[b] A parameter is proportional to the total surface area of macro pores.

[c] B parameter is proportional to the total surface area of nano pores.

[d] The pore diameter is calculated based on SAXS.

Table S3. Comparison of the ICE of various carbonaceous anode materials in SIBs.

Materials	Pyrolysis temperature (°C)	ICE	Reference
Cotton-derived carbon microtube	1600	85%	1
Banana peel-derived carbon	1400	73%	2
Sucrose-derived carbon	1300	86%	3
Hollow carbon spheres	1000	42%	4
4-shelled hard carbon nanospheres	1200	~72%	5
Charcoal-derived carbon	1900	80%	6
Pre-oxidised pitch-derived carbon	1400	89%	7
Pre-treated cellulose-derived carbon	1300	94%	8
CCD1300	1300	91%	This work

Table S4 Electrochemistry properties of carbonized CCDs and CHTCs in half cell at a current density of 30 mA g^{-1}.

Sample	ICE	ICC[a] (mAh g^{-1})	SCSC[b] (mAh g^{-1})
CCD1000	82%	266	119
CHTC1000	50%	178	125
CCD1300	91%	302	92
CHTC1300	75%	297	119
CCD1500	89%	279	72
CHTC1500	76%	298	87

[a]ICC: initial charge capacity

[b]SCSC: sloping capacity of the second cycle

Table S5 Electrochemistry properties of carbonized GCDs and GHTCs in half cell at a current density of 30 mA g^{-1}.

Sample	ICE	ICC (mAh g^{-1})
GCD1000	84%	254
GHTC1000	44%	149
GCD1300	90%	296
GHTC1300	81%	315
GCD1500	89%	288
GHTC1500	83%	315

Table S6 Elements contents of the cycled CCD1000 and CHTC1000 based on the XPS results.

Sample	C (at.%)	O (at.%)	Na (at.%)	-CO_3 (at.%)
CCD1000	59.4	28.7	11.9	6.0
CHTC1000	46.2	36.7	17.1	13.5

References

1 Y. Li, Y. S. Hu, M. M. Titirici, L. Chen and X. Huang, *Adv. Energy Mater.*, 2016, **6**, 1600659.

2 E. M. Lotfabad, J. Ding, K. Cui, A. Kohandehghan, W. P. Kalisvaart, M. Hazelton and D. Mitlin, *ACS Nano*, 2014, **8**, 7115–7129.

3 L. Xiao, H. Lu, Y. Fang, M. L. Sushko, Y. Cao, X. Ai, H. Yang and J. Liu, *Adv. Energy Mater.*, 2018, **1703238**, 1–7.

4 K. Tang, L. Fu, R. J. White, L. Yu, M. Titirici, M. Antonietti and J. Maier, *Adv. Energy Mater.*, 2012, 873–877.

5 D.-S. Bin, Y. Li, Y.-G. Sun, S.-Y. Duan, Y. Lu, J. Ma, A.-M. Cao, Y.-S. Hu and L.-J. Wan, *Adv. Energy Mater.*, 2018, **1800855**, 1800855.

6 C. Zhao, Q. Wang, Y. Lu, B. Li, L. Chen and Y. S. Hu, *Sci. Bull.*, 2018, **63**, 1125–1129.

7 Y. Lu, C. Zhao, X. Qi, Y. Qi, H. Li, X. Huang, L. Chen and Y.-S. Hu, *Adv. Energy Mater.*, 2018, **1800108**, 1800108.

8 H. Yamamoto, S. Muratsubaki, K. Kubota, M. Fukunishi, H. Watanabe, J. Kim and S. Komaba, *J. Mater. Chem. A*, 2018, **6**, 16844–16848.